Soft Matter

PAPER

View Article Online
View Journal

Cite this: DOI: 10.1039/d2sm00173j

Reshaping sub-millimetre bubbles from spheres to tori†

Xujun Zhang,*[ab] Shane Jacobeen,[c] Qiang Zhang,[d] Brian Khau,[e] Peter Yunker,[c] H. Jerry Qi,[d] Saad Bhamla*[e] and Paul S. Russo*[abf]

Received 3rd February 2022,
Accepted 22nd April 2022

DOI: 10.1039/d2sm00173j

rsc.li/soft-matter-journal

Shape-changing objects are prized for applications ranging from acoustics to robotics. We report sub-millimetre bubbles that reversibly and rapidly change not only their shape but also their topological class, from sphere to torus, when subjected to a simple pressure treatment. Stabilized by a solid-like film of nanoscopic protein "particles", the bubbles may persist in toroidal form for several days, most of them with the relative dimensions expected of Clifford tori. The ability to cross topological classes reversibly and quickly is enabled by the expulsion of protein from the strained surfaces in the form of submicron assemblies. Compared to structural modifications of liquid-filled vesicles, for example by slow changes in solution osmolality, the rapid inducement of shape changes in bubbles by application of pressure may hasten experimental investigations of surface mechanics, even as it suggests new routes to lightweight materials with high surface areas.

Introduction

Shape-changing materials are studied because of their potential in fields as diverse as frequency-optimizing antennae, soft robotic manipulators, packaging, delivery, architecture, acoustics, and medicine.[1–4] Typically, the material bends or stretches in response to an applied stimulus. Such a response is a change in the metric geometry. In contrast, certain origami folds change their topological geometry.[5] We report reversible changes of the second type, from topological sphere to torus, with both objects remaining sub-millimetre in size throughout the process.

The present study takes advantage a solid-like film composed of nearly insoluble globular protein "particles". Particulate membranes attract considerable attention for their ability to capture gases in armoured bubbles,[6–8] encase hydrophobic materials for biocatalysis,[9] and control the rheology of films of biological or geological origin.[10] Long ago, Goldacre showed that a film made from particles spread on an air-water interface often rolls up into cylindrical bubbles during surface compression, as when a flowing body of water enters a narrow channel or laps against the shore of a pond. His everyday examples included films of talc, various proteins, and the exudate of "freshly fallen autumn leaves".[11] Particles in the film reconfigure to seal the cylindrical bubbles as successive folds make contact, implying relatively weak interactions and leading Goldacre to speculate about a role of quasi-solid surface films in the formation of the first living cells. Subsequent application of vacuum tension over the suspension can reshape the cylindrical bubbles into spherical ones.[12] This process is understood as the conversion of a jammed 2D solid assembly of particles on the surface of the cylinder to a 2D gas of particles spread over the larger spherical liquid interface created during the expansion. When the partial vacuum is released, the spherical bubbles shrink and their surfaces crinkle, heralding the return of solid-like character.[12]

These steps will be illustrated below, but the focus will be on subsequent reshaping of these collapsed bubbles. We used a simple pressure treatment to convert crinkled, spherical bubbles to sub-millimetre toroidal bubbles. Toroidal structures offer the same high surface area-to-volume advantage as cylindrical ones, but in compact form. As spheres and tori belong to topologically distinct object classes, it is forbidden to transition from one to the other without tearing or merging an interface. A ball of dough cannot be reshaped into a donut without rupturing the surface at some point, which becomes the donut hole, or joining opposite ends after rolling the dough into a cylinder or mat. We observe that the sphere-to-torus transition can be repeated multiple times, and a mechanism that can enable such an unusual transition is identified.

[a] School of Materials Science and Engineering, Georgia Institute of Technology, Atlanta, GA 30332, USA. E-mail: paul.russo@mse.gatech.edu
[b] Georgia Tech Polymer Network, Georgia Institute of Technology, Atlanta, GA 30332, USA
[c] School of Physics, Georgia Institute of Technology, Atlanta, GA 30332, USA
[d] Woodruff School of Mechanical Engineering, Georgia Institute of Technology, Atlanta, GA 30332, USA
[e] School of Chemical and Biomolecular Engineering, Georgia Institute of Technology, Atlanta, GA 30332, USA. E-mail: saadb@chbe.gatech.edu
[f] School of Chemistry and Biochemistry, Georgia Institute of Technology, Atlanta, GA 30332, USA

† Electronic supplementary information (ESI) available. See DOI: https://doi.org/10.1039/d2sm00173j

The toroidal bubbles are stabilized by a thin, nearly solid film of the protein cerato-ulmin, CU (7619 g mol^{-1}), a member of the hydrophobin class of proteins produced by many species of fungi and slime molds. Hydrophobins are small ($\sim$100 amino acids) proteins that share a conserved arrangement of 4 disulfide bridges which together stabilize a globular, amphipathic structure. Sometimes referred to as nature's Janus particles,[13] hydrophobins exhibit strong surface activity. Like conventional surfactants such as sodium dodecyl sulfate, they migrate to interfaces, but with an important difference: once at an interface, they may solidify into an elastic membrane. Interfacial moduli may exceed 500 mN m^{-1}, an order of magnitude higher than observed for other proteins.[14,15] These strong membranes are known to stabilize bubbles of unusual shape;[16,17] in the case of CU, cylindrical bubbles have been observed after manual agitation of an aqueous suspension of the protein spanning a wide range of salt and pH.[12,18]

Many applications of hydrophobins are known or contemplated,[19–23] but the main reason CU is heavily studied is its longstanding association with Dutch elm disease,[24–28] "one of the worst plant diseases ever known."[29] Cherished for their beauty and strong, light wood, elm trees also play a vital role in sustaining biodiversity.[29] The possibility that pressure variations inside the tree induce bubble formation, leading to vascular embolisms that might interfere with the normal flow of water, predates quantitative knowledge of how strong the bubble membranes are.[28] Pressure variation is also a factor for hydrophobin bubbles in oceanic environments, yet a previous study[12] on that theme missed the unusual shape transformations described here and their wider implications.

Materials and methods

Protein and chemicals

Cerato-ulmin (CU) was a gift from Dr Wayne Richards of the Canadian Forest Service. Interested parties may request samples from the authors. Matrix-assisted laser desorption mass spectroscopy (MALDI-TOF) indicated a molecular weight of 7623 g mol^{-1}.[30] Fluorescein sodium salt was purchased from Sigma Aldrich and used as received. Type 1 water was supplied by a Millipore Synergy system.

Sample preparation

CU dispersion at a concentration of 0.2 mg mL^{-1} (0.13 μM) was loaded into a cell ($\sim$1 mm path length) constructed of rectangular glass tubing, which was connected to a syringe pump (Harvard Apparatus) and a differential pressure meter (Extech, model 407910). Using a 60 mL syringe, the fill and withdraw rate was 100 mL min^{-1}. (This rate, not considered optimized, was determined empirically after first observing toroidal bubbles during imprecisely controlled expansion experiments.)

Microscopy

Images and videos were taken by a standard optical microscope (Leica DM2500P or MOTIC AE31E) with a digital camera (PCO.edge). Confocal images were obtained using a Nikon A1R confocal microscope. Excitation of the sample was achieved by a 488 nm laser.

Differential dynamic microscopy

The DDM experimental setup consists of a Leica DM2500P microscope equipped with a scientific CMOS camera (PCO.edge, 1920 × 1280 pixels). A condenser lens (numerical aperture 0.9) is used to focus white light on the sample. An objective with 50× magnification (numerical aperture 0.55) is used for detection. In a typical experiment, a stack of 4000 images is acquired with a frame rate of 125 fps and an exposure time of 4 ms. To extract the dynamics of the particles, we use a DDM algorithm developed by Germain *et al.*[31] First, the intensity difference,

$$D(x, y; \Delta t) = I(x, y; t + \Delta t) - I(x, y; t) \quad (1)$$

is obtained by subtracting two images acquired at different times, where $I(x,y;t + \Delta t)$ is the intensity obtained in the sensor plane (x,y) at time t, and the minimum delay time Δt here is 0.008 s depending on the frame rate. After performing the Fourier transform of $D(x,y;\Delta t)$, one obtains

$$F_{\mathrm{D}}(u_x, u_y; \Delta t) = \int D(x, y; \Delta t) \exp\left[-i2\pi\left(u_x x + u_y y\right)\right] \mathrm{d}x\mathrm{d}y \quad (2)$$

where (u_x,u_y) are the coordinates in Fourier space. By calculating the square of the absolute value of $F_{\mathrm{D}}(u_x,u_y;\Delta t)$ and assuming the sample is isotropic, the 2D image structure function $|F_{\mathrm{D}}(q,\Delta t)|^2$ is obtained. We fitted it to

$$|F_{\mathrm{D}}(q, \Delta t)|^2 = A(q)[1 - f(q, \Delta t)] + B(q) \quad (3)$$

$$f(q, \Delta t) = \exp(-\Delta t/\tau(q)) \quad (4)$$

where $q = 2\pi\sqrt{u_x^2 + u_y^2}$ is the azimuthally averaged wave vector magnitude (suitable for comparisons to scattering experiments), $A(q)$ is the signal factor, $B(q)$ is the background, and $\tau(q)$ is the relevant q-dependent decay time. The decay rate $\Gamma(q)$ is defined as $1/\tau(q)$, and the translational diffusivity of nanoparticles $D_{\mathrm{t}} = \Gamma(q)/q^2$, is obtained by linear extrapolation to the limit $q = 0$. Hydrodynamic radii of the diffusers are then calculated using the Stokes–Einstein equation, $R_{\mathrm{h}} = kT/6\pi\eta D_{\mathrm{t}}$, where kT is the thermal energy and η is the viscosity. More theoretical background appears in a seminal DDM paper[32] and in review articles.[33,34]

Simulations

ABAQUS (ver. 6.13, Dassault Systèmes) with a dynamic explicit analysis procedure was used to simulate the collapse of spherical shells, using a symmetric geometric model and realistic parameters for CU membranes (shell thickness 2–10 nm, interfacial dilatational modulus 500 mN m^{-1}) and a Poisson ratio of 0.3. In the simulations, the radius of the spherical shell was set to a value of 30 μm that is comparable to experiments. The thickness of the shell fluctuates between the value of 10 nm and 2 nm. The location for the thickness partition is shown below. The continuum

simulations do not allow for a molecular viewpoint, such as slow surface diffusion or flow if the membranes pinch off.

Results and discussion

Understanding the sphere-to-torus transformation requires an appreciation of the reconfigurable nature of the CU membrane. We begin with a detailed look at the response of cylindrical bubbles, the progenitors of the spherical ones, to changes in air pressure above a CU-containing dispersion. This shape change from cylinder to sphere has been known for a long time,[12,18] but the time resolution achieved here permits the first detailed observation of the collapse and healing capabilities of the membrane. Suspensions of CU (0.2 mg mL^{-1}) were observed while contained in glass microscopy cells connected to a pressure system built around a syringe pump and equipped with a pressure sensor (Fig. S1, ESI†). A video camera recorded the response of the bubbles to pressure. Immediately after agitation at ambient pressure, the solution contains many rodlike bubbles (Fig. 1A). Their width varies, but slow and gentle agitation favours long and slender bubbles.[12]

As vacuum tension is applied, some bubbles buckle; see Fig. 1 and Movie S1 in the ESI.† As the two arms of the collapsed bubble are reeled in towards the expanding, smooth defect, they heal along the seam into a single protrusion, suggesting softening of the particle interactions as the film expands to its spherical shape. The solid membrane is strong enough to support the initial cylindrical shape but is easily reconfigured using air pressure above the suspension.

Now we turn to the sphere-to-torus transformation. When the vacuum tension is released, the smooth, spherical bubbles

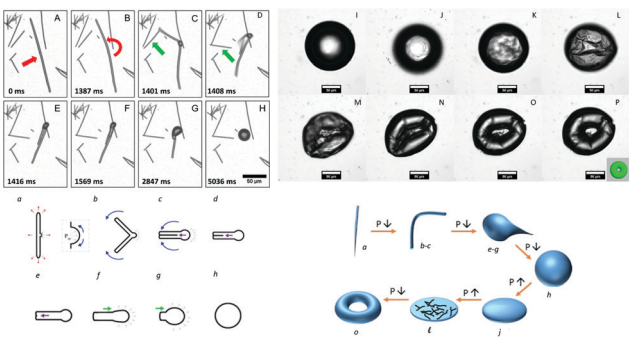

Fig. 1 Transformation of bubble geometry induced by pressure. When agitated, thin solid films on a liquid surface fold during 2D compression and pinch off to make cylinders (A). Red arrows highlight a defect that initiates collapse (A and B), which occurs too quickly to be captured by a camera operating at 137 frames per s (C and D). Green arrows show a cylindrical bubble being batted out of the way of the collapsing longer cylinder. The two collapsed arms, once in contact, heal into a single protrusion which is reeled in to create a smooth sphere near the original defect (E–H). When the vacuum is released, these surfaces return to a crinkled, 2D solid (I–L). After the crinkles appear, reapplication of vacuum tension expands the bubbles and results in creation of a smooth torus (M–P). The overall process from rod to torus is schematically shown in the lower right quadrant of the figure, where symbol P represents pressure, and the lower-case letters correspond to actual images in the remainder of the figure.

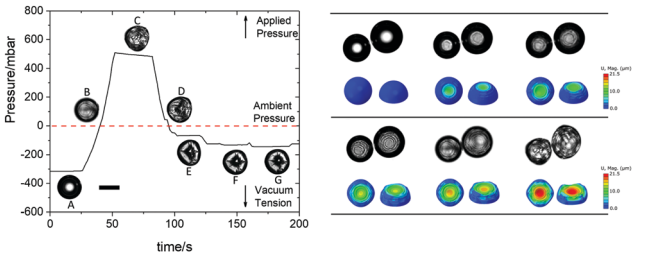

Fig. 2 Air pressure converts expanded, spherical bubbles to toroidal bubbles. At left, pressures and vacuum tensions used to reshape the bubbles (Movies S2 and S3, ESI†). The sequence begins after a smooth, spherical bubble (A) has been created by collapse and expansion of a cylindrical bubble. Applied positive pressure (B) results in crinkling (C). After ~30 s, release of the positive pressure (D) and reapplication of partial vacuum (E–G) causes the crinkled bubbles to dimple and form tori. At right, simulations using realistic moduli and nonuniform membrane thickness (ESI†) to follow the collapse (B–D) confirm the sensitivity of the spherical capsules to thickness fluctuations.[1] The simulations (colour images) only show the top half of the structures for clarity. Scale bar represents 50 μm. Colour scale corresponds to deflection, *U*, in micrometres.

develop wrinkles (Fig. 2B). Application of an overpressure, ~500 mbar, deflates and dimples these wrinkled bubbles (Fig. 2C), which float to the top of the container and touch its glass ceiling. Instead of continuing to increase the pressure, which causes full collapse of the membranes and dissolution of the bubbles, the overpressure was maintained for ~30 s before initiating a return to vacuum tension. While the pressure remains positive, the dimples become better defined (Fig. 2D). Once partial vacuum tension is achieved, the bubbles again expand, but now they assume the toroidal shape (Fig. 2D–G). The conversion of expanded, smooth spheres to crinkled spheres to tori and back can be repeated multiple times by cycling pressure (Movie S4, ESI†).

Fig. 3 collects additional micrographs to characterize the toroidal bubbles. They are numerous (Fig. 3A) and sometimes contain not just one hole (genus 1 toroid) but two or even more (genus 2 or higher) as shown in Fig. 3B and C.[35] The tori are visible in both dark-field (Fig. 3D) and confocal microscopy (Fig. 3E) and can last for several days (Fig. S2, ESI†), which is

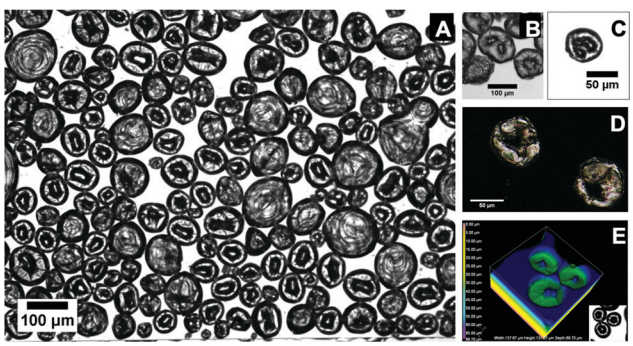

Fig. 3 CU-stabilized toroidal bubbles were observed from various optical microscopy. (A) Brightfield microscopy. (B and C) Higher-genus tori. (D) Darkfield microscopy. (E) Confocal z-stack epifluorescence (inset shows same region in brightfield illumination).

similar to collapsed spherical bubbles. After destroying all bubbles by application of ultrasonic energy, the entire process—agitation of a dilute suspension to form cylindrical bubbles; application of partial vacuum to buckle the cylindrical bubbles and create spherical ones; and vacuum release followed by re-expansion to form tori—can be repeated many times. The aqueous dispersions retain this ability for many months, a tribute to the remarkable stability of hydrophobins,[12] which are known to tolerate a wide range of temperature, pH and salt.[36]

To begin to understand toroid formation from a continuum perspective, we conducted finite-element simulations. A positive pressure load was applied to the surface of a spherical bubble, which causes the structure to shrink (Fig. 2B). We found that when the membrane thickness of the structure is set to be uniform, the structure tends to deform by denting the two ends; in contrast, when the thickness is nonuniform and has a small fluctuation (2–10 nm) along the circumferential direction of the structure (Fig. S3, ESI†), the structure first collapses at the two ends, then the collapse location progressively propagates to spread to more areas. Because of the uneven bending stiffness, a ripple-like pattern appears on the surface of the structure during the collapse. With further collapse, the structure globally buckles, and the circular equator of the structure suddenly changes into a polygonal shape. This behaviour shows good consistency with experimental observations, indicating there may be a nonuniformity in the thickness of the spherical bubbles observed in the experiments. During experimental observations of further shrinkage, the dimpled surface evolves and eventually contacts the opposite surface during the re-expansion phase. If they touch, these membranes tend to pinch off to form enclosed vesicles. This implies some fluidity in the membrane, consistent with the healing of buckled cylinders (Fig. 1E–G). If pressure is decreased at this stage, the bubble is expanded and takes a toroidal shape.

The various turbulent or sudden processes that have been reported to form toroidal gas bubbles[37–40] bear no resemblance to the quiescent pressure changes applied here, but slow squeezing of particle-armoured bubbles between plates produces genus-1 tori. This observation was attributed to the jamming of the colloidal particles on the interface.[41] A similar stabilization mechanism may apply here. It is premature to propose molecular details because the structure of CU is not yet known. The few hydrophobins whose crystal structures have been determined adopt a somewhat elongated shape with a hydrophobic patch at one end.[42–46] The high surface activity of CU certainly suggests the oily part of the molecule is firmly oriented towards the air side of the bubble, in our case the interior. The model of Prabhudesai *et al.*[47] suggests an energy input of about $100kT$, where k is Boltzmann's constant and T the Kelvin temperature, is required to detach a single protein molecule from the surface (see ESI†). The implied irreversibility of CU adsorption could contribute to the stabilization of CU air bubbles, and yet eventually CU goes back into solution (or to the glass-water interface) after the bubbles disappear, most likely in the form of aggregates. As pointed out by Hobley *et al.* in the context of a different protein surfactant,[42] the situation at the polar end of the molecule is less certain, and may depend subtly on environmental factors. One of these is surface concentration, governed by surface area, which we alter greatly during our pressure treatments. At surface concentrations supporting a film instead of a 2D gas, an odd number of protein layers is likely, in order to prevent exposure of the hydrophobic patch to an aqueous environment. Hindered redistribution of the proteins, perhaps coupled to surface-induced conformational transitions,[48] in such multilayers may supply the granular flow mechanism. Magarkar *et al.* have considered self-assembly mechanisms in 2D crystals of the hydrophobins HFBII and HFBI.[49] It is reasonable to posit that CU can undergo similar assembly.

Sub-millimetre toroidal bubbles invite comparison to liquid-filled vesicles such as liposomes and especially red blood cells, RBCs,[50,51] whose lozenge shape inspired theoretical approaches[51–53] to surface geometry that also apply to tori. A short treatment of the energetics is provided in the ESI.† Briefly, in systems lacking rapid molecular exchange mechanisms to depopulate and repopulate the membrane, the area, A, is usually taken as a constant. Non-spherical shapes can be understood as the result of more membrane area than required to enclose the volume, V. Shape is controlled not by surface energy alone, but also by the curvature energy. It is conventional to define $r_0 = (A/4\pi)^{1/2}$ as the radius of a hypothetical sphere of volume $v_0 = 4\pi(A/4\pi)^{3/2}/3$ that can be enclosed by the membrane. Various shapes are characterized by the reduced volume $v_{red} = V/v_0$. Tori are energetically favorable when $r_0 c_s < -3.9$[54,55] where c_s is the spontaneous membrane curvature (*i.e.*, inverse of the radius of the objects created by the membrane at equilibrium). Nonzero spontaneous curvature reflects asymmetry in the membrane and/or differences in the environment on either side; such differences are extreme in the case of air bubbles in water.

The low-energy branches to the shape energy equation (eqn (S5), ESI†) include tori with axial cross-sections that are sickle-shaped, discoid, and circular.[55,56] We focus on tori with circular cross-sections. As shown in Fig. 4C (inset), a circular torus is defined by its major and minor radii, R and r, respectively. When $R > r$, the structure is called a ring torus or anchor ring. When $R = r$, the structure is called a horn torus, and if $R = 0$ the torus becomes a sphere. Zhong-can *et al.*[57] first predicted the existence of toroidal vesicles whose generating circles have a R/r ratio of $\sqrt{2}$ corresponding to a (possibly degenerate) energy minimum at $v^*_{red} = 3/\left(2^{5/4}\pi^{1/2}\right) \cong 0.71$. These are called Clifford tori, and the schematic in Fig. 4C is drawn to this specification. Clifford tori were first observed in partially polymerized, liquid-in-liquid phospholipid toroidal vesicles[58] and were the most prevalent non-spherical structures. Clifford tori predominate here too. As shown in Fig. 4C, evaluation of 24 individual CU-coated toroidal bubbles revealed a mean R/r quotient of 1.40 ± 0.03 in agreement with the predicted $\sqrt{2}$.

In addition to Clifford and multi-hole tori, shapes with a single hole shifted away from the centre were found (compare Fig. 4A and B). The asymmetry of these so-called Dupin cyclides is expected on theoretical and experimental grounds.[56,58,59] It

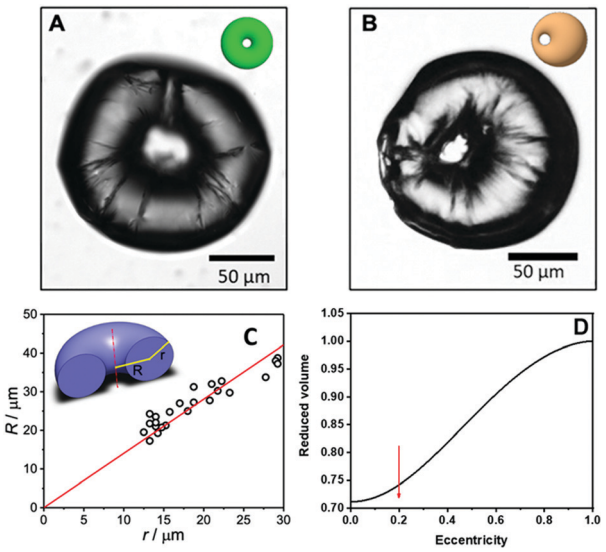

Fig. 4 Circularly symmetric and off-center tori. Cerato-ulmin can stabilize toroidal bubbles with circular cross-sections (circular tori) in axisymmetric form (A) or as asymmetric Dupin cyclides (B). *R vs. r* results for 24 individual toroidal bubbles (C); the solid line represents the theoretical prediction $R/r = \sqrt{2}$ (Clifford torus). Inset: Cutaway view of Clifford torus model. Reduced volume *vs.* eccentricity (D) predicted for Dupin cyclides (smooth curve); the arrow indicates the average of 12 asymmetric cerato-ulmin Dupin cyclide bubbles, 0.20 ± 0.03.

results because the curvature energy is nearly flat with respect to conformal transformations. Dupin cyclides are favoured by a positive Gaussian curvature modulus, although this averages to zero for genus 1 tori, and by positive or negative spontaneous curvature.[56,60] Dupin cyclides with a circular cross-section are characterized by $v_{red}^{*} < v_{red} < 1$. Just above the lower limit, the hole (handle) is slightly offset compared to a centered Clifford torus. Just below the upper limit, a small handle is located near the surface of an almost spherical object. The expectation[55] that eccentricities (as defined in Fig. S4, ESI†) will be small when v_{red} slightly exceeds v_{red}^{*} are met, as shown by the arrow for one dozen Dupin cyclides in Fig. 4D in which the smooth curve is calculated for various eccentricities according to the hypergeometric eqn (A.4) of ref. 60.

Toroidal CU-stabilized bubbles are inevitably wrinkled, meaning the membrane at rest is a thin solid, in keeping with microtensiometer measurements of curved interfaces.[61] Yet the membrane can be switched at least four times between spherical and toroidal topology (Movie S4, ESI†). The maximum number of times the membrane can be switched remains to be determined; such observations might be assisted by fluorescently labelled protein to enable surface metrology, but the strong optical gradients in these small bubbles interfere with high-resolution imaging. The available facts suggest a granular solid membrane that can flow under applied stress and repair the breakage necessary to cross topological classes. Although CU and other hydrophobins are potent surfactants, surface tension is a secondary concern for the bubbles they stabilize. In this regard, our coated bubbles are unlike those lacking a surface coating or bubbles stabilized by a liquid membrane whose constituents can exchange rapidly to the surroundings. The protein multilayer membranes that stabilize the system may reorganize and, in the process, carry off some of the gas. Precedence for that kind of shedding can be found in CU-stabilized microcapsules containing polymers in an organic solvent.[62]

Whether driven by changes in internal pressure or simply by crumbling as the solid-like membrane morphs into a new shape, "debris" is indeed visible as a blurry cloud in the vicinity of bubbles as they undergo transitions (Fig. S5, ESI†). We measured the size of the debris particles using differential dynamic microscopy, DDM, which permits diffusive measurement in a region of interest, even when the particles cannot be resolved (ESI†). The debris particles are most likely bubbles of ~400 nm radius (Fig. S6, ESI†) with wall thicknesses of about 15 nm rather than large protein aggregates.[30] The shedding of components, which creates a reservoir of partially assembled CU for repair of the structures, plus the granular flow capabilities of the membrane likely explain how it can repeatedly transition from spherical to toroidal morphology. Some unimeric protein may be present as well, but the solubility limit of CU is very low.[18]

The existence of sub-millimetre toroidal bubbles at all, let alone ones apparently at a surface energy minimum, is puzzling at first because the conditions imposed on tori compared to other non-spherical shapes are stringent.[57] CU-stabilized bubbles may seem to bear little resemblance to the various liquid-enclosing vesicles that have exhibited tori (see, *e.g.*, ref. 58). Certain similarities do exist, though. In general, the process by which the structures are formed involves disruption from a planar surface (often glass-water in the case of lipids; air-water here, but our interface has solid-like character). There is a tubular intermediate. An expansion step is involved, thus exposing the system to a wide range of quasi-equilibrium conditions to encourage interplay between structural mechanics and molecular transport. Finally, the membranes exhibit solid-like behaviour to lock in the structures that form. Yet they remain pliant; large fluctuations occur spontaneously in vesicles enclosing liquids and clearly can be induced by pressure for the surfaces surrounding CU-stabilized bubbles.

Conclusions

The finding that simple pressure treatments can reversibly transform sub-millimetre, particle-stabilized bubbles across topological classes raises the possibility that other shape changes may be achievable. Opportunities are abundant once the toroidal form has been realized because a surprisingly wide range of shapes can be fashioned from tori. A famous demonstration of this versatility is the coffee-cup-to-donut transformation[63] in which a sample of clay is made to resemble either a coffee cup or a donut while remaining a genus-1 torus. No such extreme shape transformations were observed in this work, but the variety of shapes that were observed, their easy

and rapid manipulation by pressure, and the reversibility of the sphere-to-torus transition suggest new routes to dynamic structures featuring high surface areas and light weight. Pressure manipulations of toroidal bubbles may also facilitate investigations of interfacial geometry and mechanics. Looking ahead, the greatest need is to expand the number of systems investigated, beginning with other surface-active proteins. The tools of structural biology—particularly diffraction, surface reflectometry, and NMR—may identify features that explain at a molecular level how the proteins rearrange to transform shapes. Recent studies demonstrate that shear flows can rapidly manipulate shapes too.[64] Simple systems, such as talc, identified so long ago by Goldacre[11] as having the ability to roll up into stable cylinders, should not be ignored.

Author contributions

Conceptualization: XZ, PSR. Formal analysis: XZ, BK. Methodology: XZ. Investigation: XZ, SJ, QZ. Visualization: XZ, QZ. Funding acquisition: PSR. Supervision: PSR, SB, PY, HJQ. Writing – original draft: XZ. Writing – review & editing: PSR, SB, PY, HJQ.

Conflicts of interest

There are no conflicts to declare.

Acknowledgements

We thank Karl Jacob for bending energy discussions and Jinxin Fu for DDM insights. We thank Cornelia Rosu, Bradford Blalock, and Wayne Huberty for useful discussions about CU and pressure cell design. This work was supported by the Gulf of Mexico Research Initiative (SA 12-15/GoMRI-002) through the Consortium for Molecular Engineering of Dispersant Systems (TUL-687-14/15) at Tulane University, and by a Hightower Endowment to the Georgia Tech Foundation.

Notes and references

1 J. W. Hutchinson, *Proc. R. Soc. A*, 2016, **472**, 20160577.
2 A. Kirillova and L. Ionov, *J. Mater. Chem. B*, 2019, **7**, 1597–1624.
3 K. Oliver, A. Seddon and R. S. Trask, *J. Mater. Sci.*, 2016, **51**, 10663–10689.
4 S. Li, B. Deng, A. Grinthal, A. Schneider-Yamamura, J. Kang, R. S. Martens, C. T. Zhang, J. Li, S. Yu, K. Bertoldi and J. Aizenberg, *Nature*, 2021, **592**, 386–391.
5 C. Callender and R. Weingard, *Monist*, 1996, **79**, 21–33.
6 M. Abkarian, A. B. Subramaniam, S. H. Kim, R. J. Larsen, S. M. Yang and H. A. Stone, *Phys. Rev. Lett.*, 2007, **99**, 188301.
7 S. I. Kam and W. R. Rossen, *J. Colloid Interface Sci.*, 1999, **213**, 329–339.
8 C. Buchcic, R. H. Tromp, M. B. Meinders and M. A. Cohen Stuart, *Soft Matter*, 2015, **11**, 1326–1334.
9 S. Crossley, J. Faria, M. Shen and D. E. Resasco, *Science*, 2010, **327**, 68–72.
10 G. G. Fuller and J. Vermant, *Annu. Rev. Chem. Biomol. Eng.*, 2012, **3**, 519–543.
11 R. J. Goldacre, in *Surface Phenomena in Chemistry and Biology*, ed. J. F. Danielli, K. G. A. Pankhurst and A. C. Riddiford, Pergamon, London, 1958, ch. 21, pp. 278–299.
12 X. Zhang, B. Blalock, W. Huberty, Y. Chen, F. Hung and P. S. Russo, *Langmuir*, 2019, **35**, 4380–4386.
13 M. B. Linder, *Curr. Opin. Colloid Interface Sci.*, 2009, **14**, 356–363.
14 X. Zhang, S. M. Kirby, Y. Chen, S. L. Anna, L. M. Walker, F. R. Hung and P. S. Russo, *Colloids Surf., B*, 2018, **164**, 98–106.
15 S. M. Kirby, X. Zhang, P. S. Russo, S. L. Anna and L. M. Walker, *Langmuir*, 2016, **32**, 5542–5551.
16 E. S. Basheva, P. A. Kralchevsky, K. D. Danov, S. D. Stoyanov, T. B. Blijdenstein, E. G. Pelan and A. Lips, *Langmuir*, 2011, **27**, 4481–4488.
17 H. Wosten, O. De Vries and J. Wessels, *Plant Cell*, 1993, **5**, 1567–1574.
18 P. S. Russo, F. D. Blum, J. D. Ipsen, Y. J. Abulhajj and W. G. Miller, *Can. J. Bot.*, 1982, **60**, 1414–1422.
19 B. N. Singh, B. R. Singh, V. K. Gupta, R. N. Kharwar and L. Pecoraro, *Trends Biotechnol.*, 2018, **36**, 1103–1106.
20 B. Zhang, W. Gao, J. Piao, Y. Xiao, B. Wang, W. Peng, X. Gong, Z. Wang, H. Yang and J. Chang, *ACS Appl. Mater. Interfaces*, 2018, **10**, 14549–14558.
21 C. Pigliacelli, D. Maiolo Nonappa, J. S. Haataja, H. Amenitsch, C. Michelet, P. Sanchez Moreno, I. Tirotta, P. Metrangolo and F. Baldelli Bombelli, *Angew. Chem., Int. Ed.*, 2017, **56**, 16186–16190.
22 D. Maiolo, C. Pigliacelli, P. Sanchez Moreno, M. B. Violatto, L. Talamini, I. Tirotta, R. Piccirillo, M. Zucchetti, L. Morosi, R. Frapolli, G. Candiani, P. Bigini, P. Metrangolo and F. Baldelli Bombelli, *ACS Nano*, 2017, **11**, 9413–9423.
23 H. A. Wosten and K. Scholtmeijer, *Appl. Microbiol. Biotechnol.*, 2015, **99**, 1587–1597.
24 K. J. Stevenson, J. A. Slater and S. Takai, *Phytochemistry*, 1979, **18**, 235–238.
25 M. Hubbes, *For. Chron.*, 1999, **75**, 9.
26 B. Temple, P. A. Horgen, L. Bernier and W. E. Hintz, *Fungal Genet. Biol.*, 1997, **22**, 39–53.
27 W. Richards, in *Dutch Elm Disease: Cellular and Molecular Approaches*, ed. M. B. Sticklen and J. L. Sherald, Springer-Verlag, New York, 1993, ch. 11, pp. 89–151.
28 B. Temple and P. A. Horgen, *Mycologia*, 2000, **92**, 1–9.
29 J. A. Martín, J. Sobrino-Plata, J. Rodríguez-Calcerrada, C. Collada and L. Gil, *New Forests*, 2018, **50**, 183–215.
30 A. Gorman, X. Zhang, B. Risteen, C. J. Tassone and P. S. Russo, *J. Phys. Chem. B*, 2019, **123**, 3955–3961.
31 D. Germain, M. Leocmach and T. Gibaud, *Am. J. Phys.*, 2016, **84**, 202–210.
32 R. Cerbino and V. Trappe, *Phys. Rev. Lett.*, 2008, **100**, 188102.
33 R. Cerbino and P. Cicuta, *J. Chem. Phys.*, 2017, **147**, 110901.
34 F. Giavazzi and R. Cerbino, *J. Opt.*, 2014, **16**, 083001.
35 S. A. Morris, *Topology Without Tears*, online book continuously updated (topologywithouttears.net).

36 X. Wang, J. F. Graveland-Bikker, C. G. de Kruif and G. T. Robillard, *Protein Sci.*, 2004, **13**, 810–821.
37 J. K. Walters and J. F. Davidson, *J. Fluid Mech.*, 2006, **17**, 321–336.
38 T. J. Pedley, *J. Fluid Mech.*, 2006, **32**, 97–112.
39 J. C. Bird, R. de Ruiter, L. Courbin and H. A. Stone, *Nature*, 2010, **465**, 759–762.
40 D. Préve and A. Saa, *Phys. Rev. E: Stat., Nonlinear, Soft Matter Phys.*, 2015, **92**, 042402.
41 A. Bala Subramaniam, M. Abkarian, L. Mahadevan and H. A. Stone, *Nature*, 2005, **438**, 930.
42 L. Hobley, A. Ostrowski, F. V. Rao, K. M. Bromley, M. Porter, A. R. Prescott, C. E. MacPhee, D. M. van Aalten and N. R. Stanley-Wall, *Proc. Natl. Acad. Sci. U. S. A.*, 2013, **110**, 13600–13605.
43 A. H. Kwan, R. D. Winefield, M. Sunde, J. M. Matthews, R. G. Haverkamp, M. D. Templeton and J. P. Mackay, *Proc. Natl. Acad. Sci. U. S. A.*, 2006, **103**, 3621–3626.
44 H. Fan, B. Wang, Y. Zhang, Y. Zhu, B. Song, H. Xu, Y. Zhai, M. Qiao and F. Sun, *Nat. Commun.*, 2021, **12**, 7257.
45 J. Hakanpaa, G. R. Szilvay, H. Kaljunen, M. Maksimainen, M. Linder and J. Rouvinen, *Protein Sci.*, 2006, **15**, 2129–2140.
46 J. Hakanpaa, M. Linder, A. Popov, A. Schmidt and J. Rouvinen, *Acta Crystallogr., Sect. D: Biol. Crystallogr.*, 2006, **62**, 356–367.
47 G. Prabhudesai, I. Bihi, F. Zoueshtiagh, J. Jose and M. Baudoin, *Soft Matter*, 2017, **13**, 3879–3884.
48 H. A. B. Wösten and M. L. de Vocht, *Biochim. Biophys. Acta, Rev. Biomembr.*, 2000, **1469**, 79–86.
49 A. Magarkar, N. Mele, N. Abdel-Rahman, S. Butcher, M. Torkkeli, R. Serimaa, A. Paananen, M. Linder and A. Bunker, *PLoS Comput. Biol.*, 2014, **10**, e1003745.
50 J. Käs and E. Sackmann, *Biophys. J.*, 1991, **60**, 825–844.
51 H. J. Deuling and W. Helfrich, *Biophys. J.*, 1976, **16**, 861–868.
52 P. B. Canham, *J. Theor. Biol.*, 1970, **26**, 61–81.
53 W. Helfrich, *Z. Naturforsch., C: J. Biosci.*, 1973, **28**, 693–703.
54 O. Y. Zhong-can and W. Helfrich, *Phys. Rev. A: At., Mol., Opt. Phys.*, 1989, **39**, 5280–5288.
55 U. Seifert, *Phys. Rev. Lett.*, 1991, **66**, 2404–2407.
56 F. Jülicher, U. Seifert and R. Lipowsky, *J. Phys. II*, 1993, **3**, 1681–1705.
57 O. Y. Zhong-can, *Phys. Rev. A: At., Mol., Opt. Phys.*, 1990, **41**, 4517–4520.
58 M. Mutz and D. Bensimon, *Phys. Rev. A: At., Mol., Opt. Phys.*, 1991, **43**, 4525–4527.
59 B. Fourcade, M. Mutz and D. Bensimon, *Phys. Rev. Lett.*, 1992, **68**, 2551–2554.
60 X. Michalet and D. Bensimon, *J. Phys. II*, 1995, **5**, 263–287.
61 J. D. Paulsen, E. Hohlfeld, H. King, J. Huang, Z. Qiu, T. P. Russell, N. Menon, D. Vella and B. Davidovitch, *Proc. Natl. Acad. Sci. U. S. A.*, 2016, **113**, 1144–1149.
62 C. Rosu, N. Kleinhenz, D. Choi, C. J. Tassone, X. Zhang, J. O. Park, M. Srinivasarao, P. S. Russo and E. Reichmanis, *Chem. Mater.*, 2015, **28**, 573–582.
63 V. Lucas, Mug and Torus morph.gif, **https://en.wikipedia.org/wiki/File:Mug_and_Torus_morph.gif**, **https://en.wikipedia.org/wiki/File:Mug_and_Torus_morph.gif**.
64 Q. Zhu and X. Bi, *Soft Matter*, 2022, **18**, 964–974.